

Optimal control of attitude for coupled-rigid-body spacecraft via Chebyshev-Gauss pseudospectral method*

Xinsheng GE^{1,†}, Zhonggui YI², Liquan CHEN³

1. College of Science, Beijing Information Science and Technology University, Beijing 100192, China;
2. College of Mechanical and Electrical Engineering, Beijing Information Science and Technology University, Beijing 100192, China;
3. Shanghai Institute of Applied Mathematics and Mechanics, Shanghai University, Shanghai 200072, China

Abstract The attitude optimal control problem (OCP) of a two-rigid-body spacecraft with two rigid bodies coupled by a ball-in-socket joint is considered. Based on conservation of angular momentum of the system without the external torque, a dynamic equation of three-dimensional attitude motion of the system is formulated. The attitude motion planning problem of the coupled-rigid-body spacecraft can be converted to a discrete nonlinear programming (NLP) problem using the Chebyshev-Gauss pseudospectral method (CGPM). Solutions of the NLP problem can be obtained using the sequential quadratic programming (SQP) algorithm. Since the collocation points of the CGPM are Chebyshev-Gauss (CG) points, the integration of cost function can be approximated by the Clenshaw-Curtis quadrature, and the corresponding quadrature weights can be calculated efficiently using the fast Fourier transform (FFT). To improve computational efficiency and numerical stability, the barycentric Lagrange interpolation is presented to substitute for the classic Lagrange interpolation in the approximation of state and control variables. Furthermore, numerical float errors of the state differential matrix and barycentric weights can be alleviated using trigonometric identity especially when the number of CG points is large. A simple yet efficient method is used to avoid sensitivity to the initial values for the SQP algorithm using a layered optimization strategy from a feasible solution to an optimal solution. Effectiveness of the proposed algorithm is perfect for attitude motion planning of a two-rigid-body spacecraft coupled by a ball-in-socket joint through numerical simulation.

Key words coupled rigid body, spacecraft, optimal control, pseudospectral method (PM), Chebyshev-Gauss (CG) point

Chinese Library Classification V412.4⁺2

2010 Mathematics Subject Classification 37N30

1 Introduction

With the rapid development of the science and technology of spacecraft, the control task and type of the orbited spacecraft are diversifying increasingly, and the system function and

* Received Sept. 1, 2016 / Revised Dec. 28, 2016

Project supported by the National Natural Science Foundation of China (No. 11472058)

† Corresponding author, E-mail: gebim@vip.sina.com

structure become more complicated, and lead to higher technical requirements. The model of a simple rigid body or gyrostat will no longer be used to reflect the actual mechanical model. Thus, a great number of complex models and corresponding research topics have emerged, such as multi-rigid-body systems, rigid systems with flexible attachment bodies, liquid fuels. As a kind of classic models of multi-rigid-body spacecraft, the coupled-rigid-body spacecraft can maneuver global reorientation along with the movement of the ball-in-socket joint. The coupled-rigid-body spacecraft system belongs to a type of the underactuated systems, the attitude dynamics and control of which have attracted extensive attention from researchers and scholars around the world. Krishnaprasad^[1] was the first pioneer who began to study the optimal control problem (OCP) of multi-rigid-body system in early years. Chen and Sreenath^[2] considered the controllability and control synthesis of two coupled rigid bodies with motions in space. Kolmanovsky et al.^[3] studied a system of rigid bodies interconnected by one degree of freedom (DOF) rotational joints in the planar. Reyhanoglu and McClamroch^[4] assumed that the total angular momentum of a planar rigid body system in space was zero and developed a reorientation maneuvering strategy. Fernandes et al.^[5] addressed the motion planning of coupled rigid bodies based on the Ritz approximation theory. Xia et al.^[6] investigated the problem of attitude control for a rigid spacecraft which was nonlinear in dynamics with inertia uncertainty and external disturbance by designing a sliding-mode controller. Ge and Guo^[7] used the particle swarm algorithm and spline approximation method to research the motion planning of the dual-rigid-body spacecraft. Ge and Chen^[8] researched the nonholonomic motion planning of a free-falling cat with the Gauss-Newton method based on the Ritz approximation theory.

Recently, the pseudospectral method (PM) has become a kind of important approaches to treat the OCP and nonlinear equations^[9–19]. The basic idea of the PM is that it utilizes the orthogonal polynomial to approximate state and control variables at the same time, then, an OCP can be converted to a discrete nonlinear programming (NLP) problem. Benson^[9] and Benson et al.^[10] proposed the Gauss pseudospectral method (GPM) for solving the OCP and derived strictly the costate estimate. Fahroo and Ross^[11] and Gong et al.^[12] presented the Chebyshev pseudospectral method (CPM) for directly solving a generic OCP with state and control constraints, and they gave the rigorous derivation for the costate estimate. Darby et al.^[13–14] presented an *hp*-adaptive PM for numerically solving OCPs of varying complexity. Tang et al.^[15] presented the Chebyshev-Gauss pseudospectral method (CGPM) which collocated at Chebyshev-Gauss (CG) points for direct trajectory optimization of OCPs, also they rigorously derived the costate and constraint multiplier estimates by comparing it with the Karush-Kuhn-Tucker conditions of the NLP problem. Shang and Guo^[16] adopted the CPM to study the homogeneous initial boundary value problem of a class of multi-dimensional generalized symmetric regularized long wave equations. Affy and Elgazery^[17] used the CPM to solve a set of coupled nonlinear ordinary differential equations transformed from a non-Darcy mixed convective heat and mass transfer flow. Zhuang and Huang^[18] proposed a hybrid algorithm combining the particle swarm optimization algorithm with the Legendre pseudospectral method (LPM) to solve the time-optimal trajectory planning problem of the underactuated rigid spacecraft. Huang et al.^[19] transformed the propellantless rendezvous problem of a charged spacecraft subjected to the Lorentz force about an arbitrary reference orbit into an OCP, and utilized the GPM to solve this NLP problem.

The CG points^[20] are used to substitute for Legendre-Gauss (LG) collocation points of GPM, which is the reason why the term CGPM is used. Firstly, the attitude motion planning problem of two-rigid-body spacecraft coupled by a ball-in-socket joint can be converted into a discrete NLP problem based on the CGPM theory, and then the sequential quadratic programming (SQP) algorithm is used to handle this NLP problem. Since the collocation point is the CG point, the Clenshaw-Curtis quadrature rule is presented to calculate the integral within the cost function. The corresponding quadrature weights can be calculated efficiently by the fast Fourier transform (FFT). For the aim of improving numerical stability and computational

efficiency, the barycentric Lagrange interpolation is presented to substitute for the classic Lagrange interpolation in the approximation of state and control. The trigonometric identity is used to alleviate the numerical float errors when calculating the state differential matrix and the barycentric weights. A layered optimization strategy from a feasible solution to an optimal solution is proposed to avoid sensitivity to the initial values for the SQP algorithm. At first, the SQP algorithm is used to search for a feasible solution which is satisfied by all the constraint conditions whether they are equalities or inequalities. Then, more nodes of design variables can be obtained in those feasible points with the cubic spline interpolation. At last, the SQP algorithm is used again to solve the optimal solutions as the initial values.

In this paper, a drift free nonlinear OCP of a two-rigid-body spacecraft coupled by a ball-in-socket joint is formulated based on the theory of angular momentum conservation and the principle of minimum energy control. The rationale of CGPM is presented, and the optimal control model is converted into a discrete NLP problem. A layered optimization strategy is also introduced. The results and analysis of numerical simulation are displayed, and some concluding remarks are given.

2 OCP of coupled-rigid-body spacecraft

2.1 Attitude motion model of coupled-rigid-body spacecraft

In general, the attitude of the spacecraft can be controlled by the external torques (e.g., gas jet) or the internal torques (e.g., momentum wheel). However, we consider a more interesting case of the spacecraft model that is composed of double rigid bodies by frictionless ball-in-socket joint connection in the paper (see Fig. 1). The kinematics and dynamics of each individual body are tightly coupled with the motion of the other body in the system. The spacecraft attitude control can be carried out by the hinge joint control input. Such control inputs of hinge joint preserve the system angular momentum.

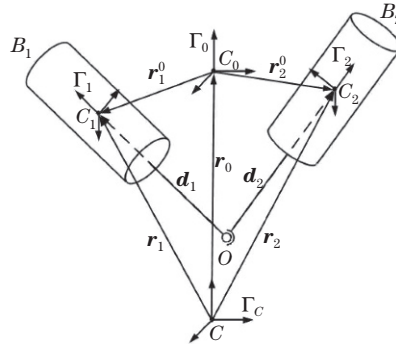


Fig. 1 Mechanical model of coupled-rigid-body spacecraft

Suppose that the system consists of rigid bodies B_i ($i = 1, 2$). The coordinate frame Γ_C is called the inertial reference frame with the origin located at the point C in space, while the coordinate frames Γ_i are called the body fixed frames to the rigid body B_i with the origin located at the mass center C_i ($i = 1, 2$), respectively.

The meaning of each symbol in Fig. 1 is as follows:

\mathbf{r}_0 , the vector from the origin C of coordinate frame Γ_C to the mass center C_0 of the system;

\mathbf{r}_1 , the vector from the origin C of coordinate frame Γ_C to the mass center C_1 of body B_1 ;

\mathbf{r}_2 , the vector from the origin C of coordinate frame Γ_C to the mass center C_2 of body B_2 ;

\mathbf{d}_1 , the vector from the ball-in-socket joint O based on Γ_1 to the mass center C_1 of body B_1 ;

\mathbf{d}_2 , the vector from the ball-in-socket joint O based on Γ_2 to the mass center C_2 of body B_2 ;

\mathbf{r}_1^0 , the vector from the mass center C_0 of system based on Γ_C to the mass center C_1 of body B_1 ;

\mathbf{r}_2^0 , the vector from the mass center C_0 of system based on Γ_C to the mass center C_2 of body B_2 ;

\mathbf{A}_1 , the coordinate transformation matrix of Γ_1 relative to Γ_C ;

\mathbf{A}_2 , the coordinate transformation matrix of Γ_2 relative to Γ_C .

In the absence of the mass of links connecting the coupled rigid bodies, it is assumed that the mass of rigid body B_i is m_i ($i = 1, 2$), and the vector of any point on the rigid body B_1 that is relative to the inertial reference frame Γ_C is \mathbf{q}_1 . Then, the kinetic energy of rigid body B_1 is given by

$$T_1 = \frac{1}{2} \int_{B_1} \|\dot{\mathbf{q}}_1(\boldsymbol{\rho}_1)\|^2 dm_1, \quad (1)$$

where $\boldsymbol{\rho}_1$ is the vector of any point on the rigid body B_1 that is relative to the body fixed frame Γ_1 . Substituting $\mathbf{q}_1 = \mathbf{r}_1 + \mathbf{A}_1 \boldsymbol{\rho}_1$ into Eq. (1) yields

$$T_1 = \frac{1}{2} \int_{B_1} \|\dot{\mathbf{r}}_1\|^2 dm_1 + \frac{1}{2} \int_{B_1} \|\dot{\mathbf{A}}_1 \boldsymbol{\rho}_1\|^2 dm_1 = \frac{1}{2} m_1 \|\dot{\mathbf{r}}_1\|^2 + \frac{1}{2} \text{tr}(\dot{\mathbf{A}}_1 \mathbf{I}_1 \dot{\mathbf{A}}_1^T), \quad (2)$$

where “tr” represents trace of square matrix. Similarly, we have the kinetic energy of rigid body B_2 ,

$$T_2 = \frac{1}{2} m_2 \|\dot{\mathbf{r}}_2\|^2 + \frac{1}{2} \text{tr}(\dot{\mathbf{A}}_2 \mathbf{I}_2 \dot{\mathbf{A}}_2^T). \quad (3)$$

In Eqs. (2) and (3), $\mathbf{I}_i = \int_{B_i} \boldsymbol{\rho}_i \boldsymbol{\rho}_i^T dm_i$ ($i = 1, 2$). Based on Eqs. (2) and (3), the kinetic energy of system can be written as follows:

$$T = T_1 + T_2 = \frac{1}{2} m_1 \|\dot{\mathbf{r}}_1\|^2 + \frac{1}{2} m_2 \|\dot{\mathbf{r}}_2\|^2 + \frac{1}{2} \text{tr}(\dot{\mathbf{A}}_1 \mathbf{I}_1 \dot{\mathbf{A}}_1^T) + \frac{1}{2} \text{tr}(\dot{\mathbf{A}}_2 \mathbf{I}_2 \dot{\mathbf{A}}_2^T). \quad (4)$$

By the theorem of motion of mass center, we have $m_1 \mathbf{r}_1^0 + m_2 \mathbf{r}_2^0 = 0$. The geometrical relationships as presented in Fig. 1 are expressed as follows:

$$\begin{cases} \mathbf{r}_1 = \mathbf{r}_0 + \mathbf{r}_1^0, \\ \mathbf{r}_2 = \mathbf{r}_0 + \mathbf{r}_2^0, \\ \mathbf{r}_2^0 = \mathbf{r}_1^0 + \mathbf{A}_1 \mathbf{d}_1 - \mathbf{A}_2 \mathbf{d}_2. \end{cases} \quad (5)$$

Additionally, $\dot{\mathbf{A}}_i \mathbf{d}_i = \mathbf{A}_i \tilde{\boldsymbol{\omega}}_i \mathbf{d}_i = -\mathbf{A}_i \tilde{\mathbf{d}}_i \boldsymbol{\omega}_i$ ($i = 1, 2$), where $\tilde{\boldsymbol{\omega}}$ and $\tilde{\mathbf{d}}$ represent the third-order skew symmetric matrices. Finally, the kinetic energy of coupled-rigid-body spacecraft can be written as

$$\begin{aligned} T &= \frac{1}{2} m \|\dot{\mathbf{r}}_0\|^2 + \frac{1}{2} \text{tr}(\boldsymbol{\omega}_1^T (\mathbf{I}_1 + \epsilon \tilde{\mathbf{d}}_1^T \tilde{\mathbf{d}}_1) \boldsymbol{\omega}_1) + \frac{1}{2} \text{tr}(\boldsymbol{\omega}_2^T (\mathbf{I}_2 + \epsilon \tilde{\mathbf{d}}_2^T \tilde{\mathbf{d}}_2) \boldsymbol{\omega}_2) \\ &\quad + \frac{1}{2} \text{tr}(\boldsymbol{\omega}_2^T \epsilon \tilde{\mathbf{d}}_2^T \mathbf{A}_2^T \mathbf{A}_1 \tilde{\mathbf{d}}_1 \boldsymbol{\omega}_1) + \frac{1}{2} \text{tr}(\boldsymbol{\omega}_1^T \epsilon \tilde{\mathbf{d}}_1^T \mathbf{A}_1^T \mathbf{A}_2 \tilde{\mathbf{d}}_2 \boldsymbol{\omega}_2) \\ &= \frac{1}{2} m \|\dot{\mathbf{r}}_0\|^2 + \frac{1}{2} \begin{bmatrix} \boldsymbol{\omega}_1^T & \boldsymbol{\omega}_2^T \end{bmatrix} \begin{bmatrix} \mathbf{J}_1 & \mathbf{J}_{12} \\ \mathbf{J}_{12}^T & \mathbf{J}_2 \end{bmatrix} \begin{bmatrix} \boldsymbol{\omega}_1 \\ \boldsymbol{\omega}_2 \end{bmatrix}, \end{aligned} \quad (6)$$

where $\mathbf{J}_i = \mathbf{I}_i + \epsilon \tilde{\mathbf{d}}_i^T \tilde{\mathbf{d}}_i$ ($i = 1, 2$), $\mathbf{J}_{12} = \epsilon \tilde{\mathbf{d}}_1^T \mathbf{A}_1^T \mathbf{A}_2 \tilde{\mathbf{d}}_2$, $m = m_1 + m_2$, and $\epsilon = m_1 m_2 / m$.

The attitude motion of the coupled-rigid-body spacecraft is considered, and the influence of the rotational motion on translational motion is ignored. It is assumed that the total angular

momentum of the system ($\mu = \frac{\partial L}{\partial \omega}$) is conserved without the external torque, where $L = T$ is the Lagrange function^[21]. Suppose that the initial value of the angular momentum is zero. Then, it would be zero all the time without the external torque. Therefore, the projection of angular momentum relative to the mass center C_0 of the system to the inertial reference frame Γ_C can be derived as

$$(\mathbf{A}_1 \mathbf{J}_1 + \mathbf{A}_2 \mathbf{J}_{12}^T) \boldsymbol{\omega}_1 + (\mathbf{A}_1 \mathbf{J}_{12} + \mathbf{A}_2 \mathbf{J}_2) \boldsymbol{\omega}_2 = \mathbf{0}. \quad (7)$$

The direction cosine matrix of the body fixed frame Γ_2 to the rigid body B_2 relative to the body fixed frame Γ_1 to the rigid body B_1 is \mathbf{A} .

The angular velocity of coordinate matrix can be expressed by the direction cosine matrix of the body fixed frame Γ_2 relative to the body fixed frame Γ_1 ,

$$\tilde{\boldsymbol{\omega}} = \mathbf{A}^T \dot{\mathbf{A}} = -\dot{\mathbf{A}}^T \mathbf{A}. \quad (8)$$

The angular velocity $\boldsymbol{\omega}_2 = \mathbf{A}^T \boldsymbol{\omega}_1 + \boldsymbol{\omega}$ of rigid body B_2 can be gained by the relationship $\mathbf{A}_2 = \mathbf{A}_1 \mathbf{A}$ and Eq. (8). Then, substituting it into Eq. (7) yields

$$\mathbf{J}_t \mathbf{A}_1 \boldsymbol{\omega}_1 = -(\mathbf{A}_1 \mathbf{J}_{12} + \mathbf{A}_2 \mathbf{J}_2) \boldsymbol{\omega}, \quad (9)$$

where $\mathbf{J}_t = \mathbf{A}_1 \mathbf{J}_1 \mathbf{A}_1^T + \mathbf{A}_2 \mathbf{J}_2 \mathbf{A}_2^T + \mathbf{A}_2 \mathbf{J}_{12}^T \mathbf{A}_1^T + \mathbf{A}_1 \mathbf{J}_{12} \mathbf{A}_2^T$ is the generalized inertia tensor of the system. Similarly, we can have the following equation of rigid body B_2 :

$$\mathbf{J}_t \mathbf{A}_2 \boldsymbol{\omega}_2 = -(\mathbf{A}_1 \mathbf{J}_1 + \mathbf{A}_2 \mathbf{J}_{12}^T) \mathbf{A} \boldsymbol{\omega}. \quad (10)$$

The two-rigid-body spacecraft coupled by a ball-in-socket joint has six DOFs. Three DOFs of them are the attitude angles of rigid body B_1 relative to the inertial reference frame Γ_C , while the rest are the attitude angles of rigid body B_2 relative to the body fixed frame Γ_1 of rigid body B_1 . In this paper, the Rodrigues parameter $\boldsymbol{\alpha} \in \mathbb{R}^3$ is used to denote the attitude angles of rigid body B_1 relative to the inertial reference frame Γ_C . Suppose $\alpha_0 = 1/(1 + \alpha^2)$, where $\alpha^2 = \boldsymbol{\alpha}^T \boldsymbol{\alpha}$. Therefore, the attitude matrix \mathbf{A}_1 can be denoted in the following form^[22]:

$$\mathbf{A}_1 = \alpha_0 \begin{bmatrix} 1 + \alpha_1^2 - \alpha_2^2 - \alpha_3^2 & 2(\alpha_1 \alpha_2 - \alpha_3) & 2(\alpha_1 \alpha_3 + \alpha_2) \\ 2(\alpha_1 \alpha_2 + \alpha_3) & 1 - \alpha_1^2 + \alpha_2^2 - \alpha_3^2 & 2(\alpha_2 \alpha_3 - \alpha_1) \\ 2(\alpha_1 \alpha_3 - \alpha_2) & 2(\alpha_2 \alpha_3 + \alpha_1) & 1 - \alpha_1^2 - \alpha_2^2 + \alpha_3^2 \end{bmatrix}. \quad (11)$$

The angular velocity of rigid body B_1 can be written as

$$\boldsymbol{\omega}_1 = \alpha_0 \begin{bmatrix} 1 & -\alpha_3 & \alpha_2 \\ \alpha_3 & 1 & -\alpha_1 \\ -\alpha_2 & \alpha_1 & 1 \end{bmatrix} \dot{\boldsymbol{\alpha}} = \mathbf{U}(\boldsymbol{\alpha}) \dot{\boldsymbol{\alpha}}. \quad (12)$$

The Rodrigues parameter $\boldsymbol{\beta} \in \mathbb{R}^3$ is also denoted for the rigid body B_2 . Then, we have

$$\boldsymbol{\omega}_2 = \beta_0 \begin{bmatrix} 1 & -\beta_3 & \beta_2 \\ \beta_3 & 1 & -\beta_1 \\ -\beta_2 & \beta_1 & 1 \end{bmatrix} \dot{\boldsymbol{\beta}} = \mathbf{U}(\boldsymbol{\beta}) \dot{\boldsymbol{\beta}}, \quad (13)$$

where β_0 has the similar definition pattern with α_0 .

The angular velocity $\mathbf{u} = [u_1, u_2, u_3]^T \in \mathbb{R}^3$ of motion of the ball-in-socket joint is treated as a pseudocontrol input. And the attitude angle of two rigid bodies is defined as the state variable which is denoted as $\mathbf{q} = [\boldsymbol{\alpha}, \boldsymbol{\beta}]^T \in \mathbb{R}^6$. Using Eqs. (12) and (13), Eqs. (9), and (10) can be written in the matrix-vector form,

$$\mathbf{G}_1(\mathbf{q}) \dot{\mathbf{q}} = \mathbf{G}_2(\mathbf{q}) \mathbf{u}, \quad (14)$$

where

$$\mathbf{G}_1(\mathbf{q}) = \begin{bmatrix} \mathbf{J}_t \mathbf{A}_1 \mathbf{U}(\boldsymbol{\alpha}) & \mathbf{0} \\ \mathbf{0} & \mathbf{J}_t \mathbf{A}_2 \mathbf{U}(\boldsymbol{\beta}) \end{bmatrix}, \quad \mathbf{G}_2(\mathbf{q}) = \begin{bmatrix} -(\mathbf{A}_1 \mathbf{J}_{12} + \mathbf{A}_2 \mathbf{J}_2) \\ (\mathbf{A}_1 \mathbf{J}_1 + \mathbf{A}_2 \mathbf{J}_{12}^T) \mathbf{A} \end{bmatrix}.$$

Since $\mathbf{G}_2(\mathbf{q})$ is nonsingular, Eq. (14) can also be written again in the form,

$$\dot{\mathbf{q}} = \mathbf{G}(\mathbf{q})\mathbf{u}, \quad (15)$$

where $\mathbf{q} \in \mathbb{R}^6$, $\mathbf{u} \in \mathbb{R}^3$, $\mathbf{G}(\mathbf{q}) = \mathbf{G}_1^{-1}(\mathbf{q})\mathbf{G}_2(\mathbf{q}) \in \mathbb{R}^{6 \times 3}$ defines a state matrix of the whole system, and Eq. (15) is the attitude nonholonomic motion equation of the rigid-body spacecraft coupled by a ball-in-socket joint.

2.2 Description of OCP

Without loss of generality, this paper takes the OCP of Bolza into account:

$$\begin{cases} \min & J = \Phi(\mathbf{x}(t_0), t_0, \mathbf{x}(t_f), t_f) + \int_{t_0}^{t_f} G(\mathbf{x}(t), \mathbf{u}(t), t) dm_1, \\ \text{subject to} & \dot{\mathbf{x}}(t) = f(\mathbf{x}(t), \mathbf{u}(t), t), \quad t \in [t_0, t_f], \\ & \phi(\mathbf{x}(t_0), t_0, \mathbf{x}(t_f), t_f) = 0, \\ & C(\mathbf{x}(t), \mathbf{u}(t), t) \leq 0, \end{cases} \quad (16)$$

where $\Phi(\cdot)$ represents the Mayer cost function, $G(\cdot)$ represents the Lagrange cost function, $f(\cdot)$ is the state equation constraint, $\phi(\cdot)$ is the initial and terminal boundary constraint, and $C(\cdot)$ is the path constraint.

Equation (15) can be treated as the control system of the coupled rigid spacecraft. According to the controllable rank condition (Chow theorem)^[23], there exists a full rank controllable Lie algebra in the control system, which can handle the attitude motion planning problem of the system by principle. We assume that there exists a solution $\mathbf{u}^* \in \mathbf{L}^2([0, T])$ in the control system, where $\mathbf{L}^2([0, T])$ is the Hilbert space of measurable vector valued functions of the form $\mathbf{u}(t)$, $t \in [0, T]$. According to the optimal control theory of minimum energy, we select the cost energy of the ball-in-socket joint as the objective function,

$$\mathbf{J}(\mathbf{u}) = \int_0^T \langle \mathbf{u}, \mathbf{u} \rangle dt, \quad (17)$$

while the state constraint equation of Bolza in Eq. (16) can be denoted by Eq. (15).

Given out the initial and terminal configurations \mathbf{q}_0 and $\mathbf{q}_f \in \mathbb{R}^6$ (namely, the state boundary constraints), the objective function can search for the pseudo-control input $\mathbf{u}(t) \in \mathbb{R}^3, t \in [0, T]^T$. Then, the attitude motion trajectory maneuvered from \mathbf{q}_0 to \mathbf{q}_f can be confirmed.

At the moment of start and shut of actuating motor controlling the motion of the ball-in-socket joint, the values of control should be zero. That is to say, $\mathbf{u}_0 = \mathbf{u}_f = \mathbf{0}$ (control boundary constraints). On the other hand, it is impossible that the output control values reach the infinite (it should have a maximum). Therefore, we are supposed to take $\|\mathbf{u}\|_\infty \leq u_{\max}$ into consideration.

3 CGPM

3.1 Rationale of CGPM

The CGPM converts the continuous OCP into a discrete parameter optimization problem contained algebraic constraints through a series of transformation, namely, the NLP problem, and it can be realized through the following steps.

(i) Time affine transformation

The CGPM should import a new time interval to convert the actual time interval $[t_0, t_f]$ of system into the interval $\tau \in [-1, 1]$, and the affine transformation can be written as

$$t = \frac{t_0 + t_f}{2} - \frac{t_0 - t_f}{2}\tau. \tag{18}$$

(ii) Variable approximation

The approximation of state and control variable CGPM takes the K CG points and $\tau_0 = -1$ as the collocation points, where the CG points are defined as follows:

$$\tau_i = \cos\left(\frac{(K + 1 - i)\pi}{K + 1}\right), \quad i = 1, 2, \dots, K. \tag{19}$$

The CG points are also called Fejér-2 or Filippi points^[24]. And the advantage of distribution over the interval $(-1,1)$ of CG points can suppress effectively the Runge phenomenon occurred in the Lagrange interpolation, which is characterized by the dense distribution on both ends and sparse distribution in the middle.

Using a basis of $(K + 1)$ th-order Lagrange interpolating polynomials to approximate the state variables,

$$\mathbf{x}(\tau) \approx \mathbf{X}(\tau) = \sum_{i=0}^K L_i(\tau)\mathbf{X}(\tau_i), \tag{20}$$

where the classic Lagrange interpolating polynomials are defined as

$$L_i(\tau) = \prod_{j=0, j \neq i}^K \frac{\tau - \tau_j}{\tau_i - \tau_j}, \quad i = 0, 1, \dots, K. \tag{21}$$

In order to improve the computational efficiency and numerical stability, the barycentric Lagrange interpolation is used to substitute for the classic Lagrange interpolation^[25],

$$L_i(\tau) = \frac{\frac{\xi_i}{\tau - \tau_i}}{\sum_{j=0}^K \frac{\xi_j}{\tau - \tau_j}}, \quad i = 0, 1, \dots, K, \tag{22}$$

where the barycentric weights ξ_i are defined as

$$\xi_i = \frac{1}{\prod_{j=0}^K (\tau_i - \tau_j)}, \quad i = 0, 1, \dots, K. \tag{23}$$

It can be found in the denominator of Eq. (23) that the calculation of $(\tau_i - \tau_j)$ would lead to floating-point cancellation errors for a large K . For this reason, an effective method is presented. Firstly, the initial and terminal point of barycentric weights ξ'_i for the CG point can be separated as follows^[25]:

$$\begin{aligned} \xi'_i &= \frac{1}{\prod_{j=0, j \neq i}^{K+1} (\tau_i - \tau_j)}, \quad i = 0, 1, \dots, K + 1 \\ &= \begin{cases} \frac{(-1)^{K+1-i}}{2}, & i = 0, K + 1, \\ (-1)^{K+1-i}, & i = 1, 2, \dots, K. \end{cases} \end{aligned} \tag{24}$$

By comparing Eq. (23) with Eq. (24), it can be seen that ξ_i is equal to ξ'_i when the denominator is $i = K$. Therefore, using the trigonometric identity and considering $\tau_0 = -1$ and $\tau_{K+1} = 1$, Eq. (23) can be expressed again in another form as

$$\begin{aligned} \xi_i &= (\tau_i - \tau_{K+1})\xi'_i = (\tau_i - 1)\xi'_i \\ &= \begin{cases} (\tau_0 - 1)\xi'_0 = -2\xi'_0, & i = 0, \\ \left(\cos\left(\frac{(K+1-i)\pi}{K+1}\right) - 1\right)\xi'_i, & i = 1, 2, \dots, K \end{cases} \\ &= \begin{cases} (-1)^K, & i = 0, \\ (-1)^{K-i}2\sin^2\left(\frac{(K+1-i)\pi}{2(K+1)}\right), & i = 1, 2, \dots, K. \end{cases} \end{aligned} \tag{25}$$

There is no derivative of control in the CGPM. Therefore, the approximation of control is simpler than the state variables. For consistency in the form, CG points are selected as collocation points for the CGPM, and the K th-order barycentric Lagrange interpolating polynomials $\bar{L}_i(\tau)$ ($i = 1, 2, \dots, K$) are used as basis functions to approximate the control variables,

$$\mathbf{u}(\tau) \approx \mathbf{U}(\tau) = \sum_{i=1}^K \bar{L}_i(\tau)\mathbf{U}(\tau_i). \tag{26}$$

(iii) Transformation of dynamic differential equation

In the PM, the state variables are approximated by global orthogonal polynomials. Therefore, the time derivative of them can be derived by Eq. (20),

$$\dot{\mathbf{x}}(\tau_k) \approx \dot{\mathbf{X}}(\tau_k) = \sum_{i=0}^K \dot{L}_i(\tau_k)\mathbf{X}(\tau_i), \tag{27}$$

where the classic Lagrange interpolating polynomials can be denoted by a differential matrix $\mathbf{D} \in \mathbb{R}^{K \times (K+1)}$ as

$$D_{ki} = \dot{L}_i(\tau_k) = \sum_{l=0, l \neq i}^K \frac{\prod_{j=0, j \neq i, l}^K (\tau_k - \tau_j)}{\prod_{j=0, j \neq i}^K (\tau_i - \tau_j)}. \tag{28}$$

Since barycentric Lagrange interpolating is used in this paper, the differential matrix should be given by Eq. (29). It has a better numerical stability than Eq. (28)^[26],

$$D_{ki} = \begin{cases} \frac{\xi_i}{\xi_k} \frac{1}{\tau_k - \tau_i}, & k \neq i, \\ -\sum_{j=0, j \neq k}^K D_{kj}, & k = i, \end{cases} \tag{29}$$

where $k = 1, 2, \dots, K$, and $i = 0, 1, \dots, K$. Substituting Eq. (29) into the dynamics equation yields the following discrete form:

$$\sum_{i=0}^K D_{ki}\mathbf{X}_i - \frac{t_f - t_0}{2}f(\mathbf{X}_k, \mathbf{U}_k, \tau_k; t_0, t_f) = 0, \quad k = 1, 2, \dots, K. \tag{30}$$

It can also be found in the denominator of the first row in Eq. (29) that the calculation of $(\tau_k - \tau_i)$ will lead to floating-point cancellation errors. On the other hand, τ_i (see Eq. (19)) is a triangle cosine function. For these reasons, the trigonometric identity is used to avoid phenomena and yield Eq. (31). While ξ_i and ξ_k of Eq. (29) can be calculated efficiently by Eq. (25),

$$\begin{aligned}\tau_k - \tau_i &= \cos\left(\frac{(K+1-k)\pi}{K+1}\right) - \cos\left(\frac{(K+1-i)\pi}{K+1}\right) \\ &= 2\sin\left(\frac{(k+i)\pi}{2(K+1)}\right)\sin\left(\frac{(k-i)\pi}{2(K+1)}\right).\end{aligned}\quad (31)$$

(iv) Terminal constraint of state

It is known in the Bolza OCP (see Eq. (16)) that the state equations contain terminal constraints. However, the time interval of Eq. (20) is $[-1, 1]$. Thus, the approximated state does not include the terminal state $\mathbf{X}(\tau_f)$. Therefore, the integration of the dynamics equation over the time interval $[-1, 1]$ yields

$$\int_{-1}^1 \dot{\mathbf{x}}(\tau) d\tau = \frac{t_f - t_0}{2} \int_{-1}^1 f(\mathbf{x}(\tau), \mathbf{u}(\tau), \tau) d\tau. \quad (32)$$

The Clenshaw-Curtis quadrature rules are used to substitute for Gauss quadrature in the approximation of Eq. (32)^[27],

$$\mathbf{X}_f = \mathbf{X}_0 + \frac{t_f - t_0}{2} \sum_{k=1}^K \mu_k^{\text{cc}} f(\mathbf{X}_k, \mathbf{U}_k, \tau_k; t_0, t_f). \quad (33)$$

The direct expansion of the left side of Eq. (32) can gain a linear result. The nonlinear terms in Eq. (33) are commonly used in the GPM^[9-10,14]. However, the former has a better computational efficiency than the latter, and the linear result can be written as

$$\begin{aligned}\mathbf{X}_f &= \mathbf{X}_0 + \int_{-1}^1 \dot{\mathbf{x}}(\tau) d\tau = \mathbf{X}_0 + \int_{-1}^1 \sum_{i=0}^K \dot{L}_i(\tau) \mathbf{X}(\tau_i) d\tau \\ &= \mathbf{X}_0 + \sum_{i=0}^K \mathbf{X}(\tau_i) \int_{-1}^1 \dot{L}_i(\tau) d\tau = \mathbf{X}_0 + \sum_{i=0}^K \mathbf{X}(\tau_i) \left(\sum_{k=1}^K \mu_k^{\text{cc}} \dot{L}_i(\tau_k) \right) \\ &= \mathbf{X}_0 + \sum_{i=0}^K \mathbf{X}(\tau_i) \sum_{k=1}^K \mu_k^{\text{cc}} D_{ki},\end{aligned}\quad (34)$$

where τ_k presents the CG point. And μ_k^{cc} denotes Clenshaw-Curtis quadrature weights which can be efficiently and numerically stable by using the FFT^[28],

$$\mu_k^{\text{cc}} = \begin{cases} \mu_k^{f_2} + \frac{c_k(-1)^k}{(K+1)^2 - 1} & \text{for } (K+1) \text{ is even,} \\ \mu_k^{f_2} + \frac{c_k(-1)^k}{(K+1)^2} \cos\left(\frac{k\pi}{K+1}\right) & \text{for } (K+1) \text{ is odd,} \end{cases} \quad (35)$$

where c_k is defined by

$$c_k = \begin{cases} 1, & k = 0 \quad \text{or} \quad k = K+1, \\ 2, & \text{otherwise,} \end{cases} \quad (36)$$

and $\mu_k^{f_2}$ represents the Fejér-2 quadrature weight,

$$\mu_k^{f_2} = F_{K+1}^{-1} \nu_k, \tag{37}$$

where F_{K+1}^{-1} represents the inverse FFT (IFFT), and ν_k is defined as follows:

$$\begin{cases} \nu_k = \frac{2}{1-4k^2}, & k = 0, 1, \dots, \left[\frac{K+1}{2}\right] - 1, \\ \nu_{\lfloor (K+1)/2 \rfloor} = \frac{K-2}{2\lfloor (K+1)/2 \rfloor - 1}, \\ \nu_{K+1-k} = \nu_k, & k = 1, 2, \dots, \left[\frac{K}{2}\right]. \end{cases} \tag{38}$$

Finally, we assume that $\mu_{K+1}^{f_2} = \mu_0^{f_2} = 0$ and $\mu_{K+1}^{cc} = \mu_0^{cc}$. And we take the real part after calculating Eq. (37).

(v) Objective function

Utilizing the Clenshaw-Curtis quadrature rules to approximate the integral part of Bolza OCP (see Eq. (16)) yields the following equation:

$$J = \Phi(\mathbf{X}_0, t_0, \mathbf{X}_f, t_f) + \frac{t_f - t_0}{2} \sum_{k=1}^K \mu_k^{cc} g(\mathbf{X}_k, \mathbf{U}_k, \tau_k; t_0, t_f). \tag{39}$$

3.2 NLP problem

In this section, we utilize the CGPM to convert the OCP of the coupled-rigid-body spacecraft into a discrete NLP problem. Firstly, we should define the state variables of each collocation point as $\mathbf{X}_{1K}, \mathbf{X}_{2K}, \mathbf{X}_{3K}, \mathbf{X}_{4K}, \mathbf{X}_{5K}, \mathbf{X}_{6K} \in \mathbb{R}^{K+1}$, the control variables as $\mathbf{U}_{1K}, \mathbf{U}_{2K}, \mathbf{U}_{3K} \in \mathbb{R}^K$. Then, the discrete approximated cost function is given by

$$J = \frac{t_f - t_0}{2} (\boldsymbol{\mu}^{cc})^T (\mathbf{U}_{1K}^2 + \mathbf{U}_{2K}^2 + \mathbf{U}_{3K}^2), \tag{40}$$

where $\boldsymbol{\mu}^{cc}$ is a sequence of Clenshaw-Curtis quadrature weights.

Using the differential approximated matrix to denote the discrete state equation in the form of matrix expression,

$$\begin{cases} D\mathbf{X}_{1K} - \frac{t_f - t_0}{2} (\mathbf{G}_{11}\mathbf{U}_{1K} + \mathbf{G}_{12}\mathbf{U}_{2K} + \mathbf{G}_{13}\mathbf{U}_{3K}) = \mathbf{0}, \\ D\mathbf{X}_{2K} - \frac{t_f - t_0}{2} (\mathbf{G}_{21}\mathbf{U}_{1K} + \mathbf{G}_{22}\mathbf{U}_{2K} + \mathbf{G}_{23}\mathbf{U}_{3K}) = \mathbf{0}, \\ D\mathbf{X}_{3K} - \frac{t_f - t_0}{2} (\mathbf{G}_{31}\mathbf{U}_{1K} + \mathbf{G}_{32}\mathbf{U}_{2K} + \mathbf{G}_{33}\mathbf{U}_{3K}) = \mathbf{0}, \\ D\mathbf{X}_{4K} - \frac{t_f - t_0}{2} (\mathbf{G}_{41}\mathbf{U}_{1K} + \mathbf{G}_{42}\mathbf{U}_{2K} + \mathbf{G}_{43}\mathbf{U}_{3K}) = \mathbf{0}, \\ D\mathbf{X}_{5K} - \frac{t_f - t_0}{2} (\mathbf{G}_{51}\mathbf{U}_{1K} + \mathbf{G}_{52}\mathbf{U}_{2K} + \mathbf{G}_{53}\mathbf{U}_{3K}) = \mathbf{0}, \\ D\mathbf{X}_{6K} - \frac{t_f - t_0}{2} (\mathbf{G}_{61}\mathbf{U}_{1K} + \mathbf{G}_{62}\mathbf{U}_{2K} + \mathbf{G}_{63}\mathbf{U}_{3K}) = \mathbf{0}, \end{cases} \tag{41}$$

where \mathbf{G}_{ij} ($i = 1, 2, \dots, 6$, and $j = 1, 2, 3$) are the units of state matrix in Eq. (15).

Also, the terminal constraints of state are given by

$$\begin{cases} X_{1f} - X_{10} - \frac{t_f - t_0}{2} (\boldsymbol{\mu}^{cc})^T (\mathbf{G}_{11}\mathbf{U}_{1K} + \mathbf{G}_{12}\mathbf{U}_{2K} + \mathbf{G}_{13}\mathbf{U}_{3K}) = 0, \\ X_{2f} - X_{20} - \frac{t_f - t_0}{2} (\boldsymbol{\mu}^{cc})^T (\mathbf{G}_{21}\mathbf{U}_{1K} + \mathbf{G}_{22}\mathbf{U}_{2K} + \mathbf{G}_{23}\mathbf{U}_{3K}) = 0, \\ X_{3f} - X_{30} - \frac{t_f - t_0}{2} (\boldsymbol{\mu}^{cc})^T (\mathbf{G}_{31}\mathbf{U}_{1K} + \mathbf{G}_{32}\mathbf{U}_{2K} + \mathbf{G}_{33}\mathbf{U}_{3K}) = 0, \\ X_{4f} - X_{40} - \frac{t_f - t_0}{2} (\boldsymbol{\mu}^{cc})^T (\mathbf{G}_{41}\mathbf{U}_{1K} + \mathbf{G}_{42}\mathbf{U}_{2K} + \mathbf{G}_{43}\mathbf{U}_{3K}) = 0, \\ X_{5f} - X_{50} - \frac{t_f - t_0}{2} (\boldsymbol{\mu}^{cc})^T (\mathbf{G}_{51}\mathbf{U}_{1K} + \mathbf{G}_{52}\mathbf{U}_{2K} + \mathbf{G}_{53}\mathbf{U}_{3K}) = 0, \\ X_{6f} - X_{60} - \frac{t_f - t_0}{2} (\boldsymbol{\mu}^{cc})^T (\mathbf{G}_{61}\mathbf{U}_{1K} + \mathbf{G}_{62}\mathbf{U}_{2K} + \mathbf{G}_{63}\mathbf{U}_{3K}) = 0. \end{cases} \tag{42}$$

Finally, the initial and terminal constraints of state and control, as well as the control constraints, are set as

$$\begin{cases} \mathbf{q}_0 - \mathbf{X}_0 = \mathbf{0}, & \mathbf{q}_f - \mathbf{X}_f = \mathbf{0}, \\ \mathbf{u}_0 - \mathbf{U}_0 = \mathbf{0}, & \mathbf{u}_f - \mathbf{U}_f = \mathbf{0}, \\ |\mathbf{U}| \leq U_{\max}, \end{cases} \quad (43)$$

where \mathbf{X}_0 and \mathbf{X}_f represent the first and last columns of the approximated state, respectively, and it is the same with \mathbf{U}_0 and \mathbf{U}_f . Here, U_{\max} denotes the control maximum.

From Eqs. (40)–(43), a general NLP problem of the OCP can be expressed as

$$\begin{cases} \min & J = F(\mathbf{y}), \\ \text{subject to} & h_i(\mathbf{y}) = 0, \quad i = 1, 2, \dots, 6K + 6 + 18, \\ & g_i(\mathbf{y}) \leq 0, \quad i = 1, 2, \dots, 3K, \end{cases} \quad (44)$$

where \mathbf{y} represents the design variables containing state variables and control variables.

3.3 Optimization strategy and process

Theoretically, we can obtain the attitude trajectories of the coupled-rigid-body spacecraft by employing the SQP algorithm.

However, the actual troubles are that the number of design variables is huge when large CG points are chosen. For example, when we take 60 CG points, there will be 558 design variables. For so many design variables, it is difficult for us to set the initial guess values for the SQP, and if the inappropriate initial values are used, we may not get a feasible solution for the SQP algorithm. In addition, the SQP algorithm does not possess the capability to search for a global optimal solution. It depends on the initial values. Generally, it only can converge to a local optimal solution that is close to the initial value. Given these reasons, a layered optimization strategy is proposed as follows.

(i) Calculating feasible solution

The essences of a feasible solution are that it does not search for the optimal solution which is satisfied with all constraint conditions (including equality and inequality constraints), and that it does not consider the actual cost function. Contrarily, it treats the converted equality constraints as the new pseudo-objective function. Therefore, the new NLP problem does not contain equality constraints, and it can be obtained from Eq. (44),

$$\begin{cases} \min & J = \text{sqrt}\left(\sum_{i=1}^{6K+24} h_i^2(\mathbf{y})\right), \\ \text{subject to} & g_i(\mathbf{y}) \leq 0, \quad i = 1, 2, \dots, 3K. \end{cases} \quad (45)$$

Since the PM method can obtain the higher solution accuracy at lower nodes, also, it has lower sensitivity to initial values and has fewer design variables at this time, we are supposed intensively to choose fewer nodes $K1$, and utilize the SQP algorithm of the toolbox of MATLAB to obtain a feasible solution.

(ii) Calculating optimal solution

Take the discrete solution gained from the first step as the interpolating nodes of cubic spline interpolation, and then we can get more CG points by applying these discrete scaled time CG points into the spline function. In other words, $K2$ initial values are yielded by $K1$ interpolating nodes. Then, the optimal solution can be achieved now by substituting the $K2$ initial values into the SQP algorithm to search for the NLP problem (see Eq. (44)).

The layered optimization strategy is presented in Fig. 2.

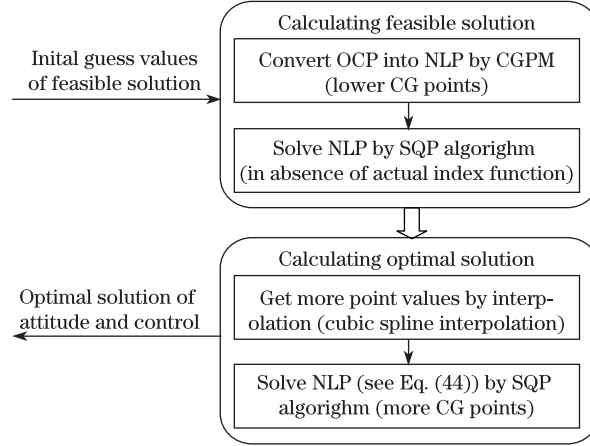


Fig. 2 Flow chart of attitude optimization for coupled-rigid-body spacecraft via CGPM

4 Results of numerical simulation

In this section, the attitude motion planning problems of the two-rigid-body spacecraft coupled by a ball-in-socket joint are numerically simulated. The mass and geometric parameters of the system are given as follows: $m_1 = m_2 = 2$ kg, $\mathbf{d}_1 = \mathbf{d}_2 = [0, 0, 1]$, and

$$\mathbf{I}_1 = \mathbf{I}_2 = \text{diag}(2, 3, 4) \text{ kg} \cdot \text{m}^2.$$

The initial and terminal attitudes of the system, as well as the control constraints, are given as

$$\begin{cases} \mathbf{q}_0 = [0.0663, 0.3142, 0.5465, -0.0663, -0.3142, 0.5465]^T, \\ \mathbf{q}_f = [-0.0663, 0.3142, -0.5465, 0.0663, -0.3142, -0.5465]^T, \\ \mathbf{u}_0 = \mathbf{u}_f = [0, 0, 0]^T, \quad U_{\max} = 0.5. \end{cases}$$

The layered optimization strategy is adopted during the optimization. Here, 6 CG points are selected for the feasible solution and 60 CG points for the optimal solution. Set the maneuver time $T = 5$ s. After simulating, the curves of the optimal solution are shown in Figs. 3, 4, and 5, where the circles denote the CG points of the optimal solution. In Fig. 3, the black solid line denotes the attitude trajectory of rigid body B_1 . Similarly, the black solid line in Fig. 4 denotes the attitude trajectory of rigid body B_2 . The start and end points of curves represent the initial and terminal attitude configurations, respectively. Moreover, Fig. 5 provides the curve of pseudo-control input. It is obvious that the start and end points of control curve are zero. Therefore, this solution can satisfy the requirements of zero boundary control at the moment of start and shut of actuating motor perfectly. Moreover, the control can switch between the minimal and maximal control values.

In order to validate the attitude curves, the control values in Fig. 5 are applied to Eq. (15) with the integral operation which is the fourth-order and fifth-order Runge-Kutta method. The results of integral operation are shown in Figs. 3 and 4 in the form of black dotted lines. As seen in the local enlarged figures, the integral curves from ODE45 almost overlap with the curves by the CGPM. Therefore, it is rational and valid.

For showing intuitively and comparing the feature of the CGPM, this paper also presents the calculation results of GPM. The collection points of GPM are LG points, the GPM utilizes the Gaussian quadrature to approximate the integration item in the index function, also, it uses the classic Lagrange interpolation to approximate state and control variables, and it makes use of the nonlinear terms in Eq. (33) to compute the terminal constraints of the states. The GPM also makes use of the layered optimization strategy, and the setting of related parameters is similar to

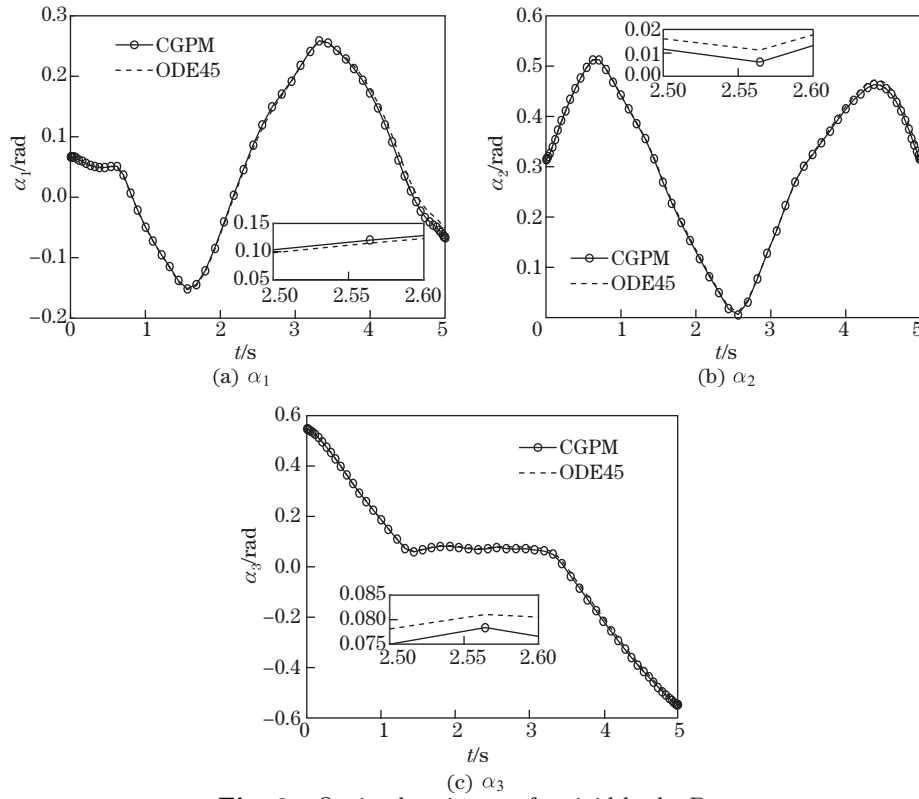


Fig. 3 Optimal trajectory for rigid body B_1

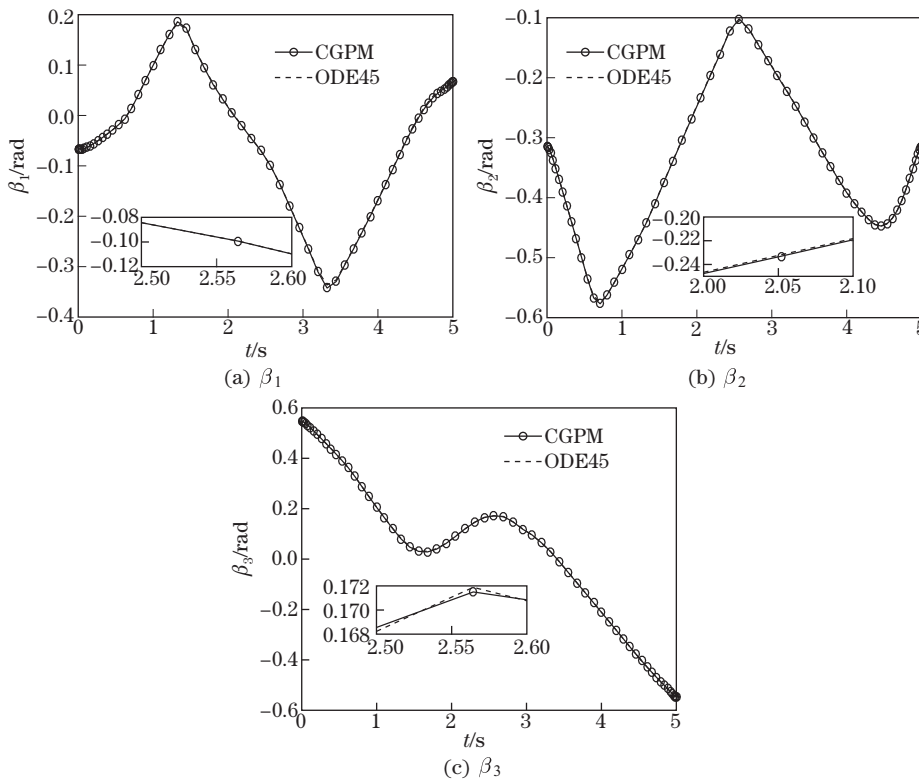


Fig. 4 Optimal trajectory for rigid body B_2

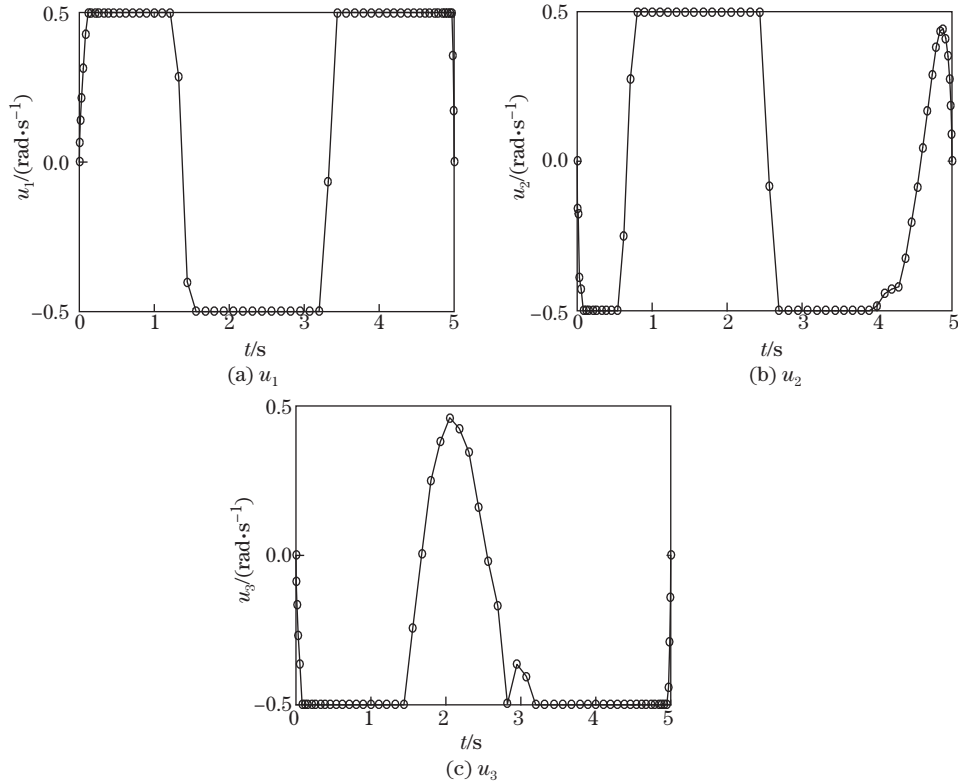


Fig. 5 Optimal control input for ball-in-socket joint model

the CGPM. The initial guess values of the feasible solution for both CGPM and GPM are created randomly by the “rand” function included in MATLAB. The data are recorded in Table 1, which are gained by calculating the mean of the 6th running results. In Table 1, the parameters $t_{d,f}$, J_f , and n_{\max} denote the iterating time, the value of object function, and the maximal absolute value of inequality constraints after solving the feasible solutions, respectively. $t_{d,o}$ and J_o are the iterating time and the objective function value of the optimal solution, respectively. Finally, the parameter A_e represents the maximum absolute error of terminal attitude, and T_{CPU} denotes the whole running time. It can be seen that the objective function value of CGPM is smaller than the one of GPM for both the feasible solution and the optimal solution. The running time of CGPM is half of the one with the GPM. The terminal attitude has already a very high accuracy 10^{-14} of the maximal absolute error, and the CGPM can also reach this level easily. Thus, the comparisons in Table 1 can embody intuitively that the CGPM adopted in this paper has the higher computational efficiency and solving accuracy.

Table 1 Comparisons for CGPM and GPM

Method	$t_{d,f}$	J_f	n_{\max}	$t_{d,o}$	J_o	$A_e/(\times 10^{-14})$	T_{CPU}/s
CGPM	17	0.006 7	0.500 0	128.333 3	3.285 7	7.529 2	111.267 0
GPM	17	0.008 3	0.500 0	127.833 3	3.338 7	4.837 0	229.241 3

5 Conclusions

In this paper, the CG points are used to substitute for the LG collocation points of GPM. Thus, the method is called the CGPM. Firstly, the attitude motion planning problem of two-rigid-body-spacecraft coupled by a ball-in-socket joint can be converted into a discrete NLP

problem based on the CGPM theory. Then, the SQP algorithm is used to handle this NLP problem. Moreover, a layered optimization strategy from a feasible solution to an optimal solution is proposed to avoid sensitivity to the initial values for the SQP algorithm. A set of simple yet efficient methods are used to improve the numerical stability and computational efficiency and avoid the floating-point cancellation errors. The results of numerical simulation and analysis in this paper show the following conclusions: (i) The nonlinear control problem of the coupled-rigid-body spacecraft can be converted into a motion programming problem of draft free system; (ii) In absence of the external torque, the rotation motion of the joint interconnecting the two-rigid-body can maneuver the motion of the whole system; (iii) The optimal control can meet the requirements of zero boundary control, and switch between the minimal and maximal control values; (iv) The inverse integration demonstrates that the attitude curves are rational and effective; (v) The comparison between CGPM and GPM indicates that the CGPM has the higher computational efficiency. The method adopted in this paper provides another fast and efficient approach for solving problems of direct trajectory optimization and attitude optimization.

References

- [1] Krishnaprasad, P. S. Geometric phases and optimal reconfiguration for multibody systems. *American Control Conference*, **1990**, 2440–2444 (1990)
- [2] Chen, C. K. and Sreenath, N. Control of coupled spatial two-body systems with nonholonomic constraints. *IEEE Conference on Decision and Control*, **2**, 949–954 (1993)
- [3] Kolmanovsky, I., McClamroch, N. H., and Coppola, V. T. New results on control of multibody systems which conserve angular momentum. *Journal of Dynamical and Control Systems*, **1**, 447–462 (1995)
- [4] Reyhanoglu, M. and McClamroch, N. H. Planar reorientation maneuvers of space multibody systems using internal controls. *Journal of Guidance Control and Dynamics*, **15**, 1475–1480 (1992)
- [5] Fernandes, C., Gurvits, L., and Li, Z. X. Near-optimal nonholonomic motion planning for a system of coupled rigid bodies. *IEEE Transactions on Automatic Control*, **39**, 450–463 (1994)
- [6] Xia, Y. Q., Zhu, Z., Fu, M. Y., and Wang, S. Attitude tracking of rigid spacecraft with bounded disturbances. *IEEE Transactions on Industrial Electronics*, **58**, 647–659 (2011)
- [7] Ge, X. S. and Guo, Z. X. Attitude motion planning of dual rigid bodies spacecraft using spline approximation. *Scientia Sinica Physica Mechanica and Astronomica*, **43**, 407–414 (2013)
- [8] Ge, X. S. and Chen, L. Q. Optimal control of nonholonomic motion planning for a free-falling cat. *Applied Mathematics and Mechanics (English Edition)*, **28**, 601–607 (2007) DOI 10.1007/s10483-007-0505-z
- [9] Benson, D. A. *A Gauss Pseudospectral Transcription for Optimal Control*, Ph. D. dissertation, Massachusetts Institute of Technology, Cambridge, 1–243 (2005)
- [10] Benson, D. A., Huntington, G. T., Thorvaldsen, T. P., and Rao, A. V. Direct trajectory optimization and costate estimation via an orthogonal collocation method. *Journal of Guidance Control and Dynamics*, **29**, 1435–1439 (2006)
- [11] Fahroo, F. and Ross, I. M. Direct trajectory optimization by a Chebyshev pseudospectral method. *Journal of Guidance Control and Dynamics*, **25**, 160–166 (2002)
- [12] Gong, Q., Ross, I. M., and Fahroo, F. Costate computation by a Chebyshev pseudospectral method. *Journal of Guidance Control and Dynamics*, **33**, 623–628 (2010)
- [13] Darby, C. L., Hager, W. W., and Rao, A. V. An *hp*-adaptive pseudospectral method for solving optimal control problems. *Optimal Control Applications and Methods*, **32**, 476–502 (2011)
- [14] Darby, C. L., Hager, W. W., and Rao, A. V. Direct trajectory optimization using a variable low-order adaptive pseudospectral method. *Journal of Spacecraft and Rockets*, **48**, 433–445 (2011)
- [15] Tang, X. J., Wei, J. L., and Chen, K. A Chebyshev-Gauss pseudospectral method for solving optimal control problems. *Acta Automatica Sinica*, **41**, 1778–1787 (2015)

-
- [16] Shang, Y. D. and Guo, B. L. Analysis of Chebyshev pseudospectral method for multi-dimensional generalized SRLW equations. *Applied Mathematics and Mechanics (English Edition)*, **24**, 1168–1183 (2003) DOI 10.1007/BF02438106
- [17] Afify, A. A. and Elgazery, N. S. Effect of double dispersion on non-Darcy mixed convective flow over vertical surface embedded in porous medium. *Applied Mathematics and Mechanics (English Edition)*, **34**, 1247–1262 (2013) DOI 10.1007/s10483-013-1742-6
- [18] Zhuang, Y. F. and Huang, H. B. Time-optimal trajectory planning for underactuated spacecraft using a hybrid particle swarm optimization algorithm. *Acta Astronautica*, **94**, 690–698 (2014)
- [19] Huang, X., Yan, Y., Zhou, Y., and Zhang, H. Pseudospectral method for optimal propellant-less rendezvous using geomagnetic Lorentz force. *Applied Mathematics and Mechanics (English Edition)*, **36**, 609–618 (2015) DOI 10.1007/s10483-015-1936-7
- [20] Broutman, D. A practical guide to pseudospectral methods. *Journal of Fluid Mechanics*, **360**, 375–378 (1998)
- [21] Fernandes, C., Gurvits, L., and Li, Z. X. Attitude control of a space platform/manipulator system using internal motion. *International Journal of Robotics Research*, **13**, 289–304 (1994)
- [22] Shabana, A. A. *Dynamics of Multibody Systems*, 4th ed., Cambridge University Press, Cambridge, 58–59 (2013)
- [23] Isidori, A. *Nonlinear Control Systems II*, Springer-Verlag, Berlin, 1–74 (1999)
- [24] Weideman, J. and Trefethen, L. The kink phenomenon in Fejér and Clenshaw-Curtis quadrature. *Numerische Mathematik*, **107**, 707–727 (2007)
- [25] Berrut, J. P. and Trefethen, L. N. Barycentric Lagrange interpolation. *SIAM Review*, **46**, 501–517 (2004)
- [26] Costa, B. and Don, W. S. On the computation of high order pseudospectral derivatives. *Applied Numerical Mathematics*, **33**, 151–159 (2000)
- [27] Trefethen, L. N. Is Gauss quadrature better than Clenshaw-Curtis? *SIAM Review*, **50**, 67–87 (2008)
- [28] Waldvogel, J. Fast construction of the Fejér and Clenshaw-Curtis quadrature rules. *BIT Numerical Mathematics*, **46**, 195–202 (2006)